materials

MDPI

Communication

Investigation of Cation Exchange Behaviors of $FA_xMA_{1-x}PbI_3$ Films Using Dynamic Spin-Coating

HyangMi Yu [1,†], Byeong-Geun Jeong [1,†], Dae-Young Park [2], Seong-Chu Lim [1,3,*], Gon Namkoong [1,4,*] and Mun-Seok Jeong [2,5,*]

[1] Department of Energy Science, Sungkyunkwan University, Suwon 16419, Korea; gidal0072@skku.edu (H.Y.); zinzza228@skku.edu (B.-G.J.)
[2] Department of Physics, Hanyang University, Seoul 04763, Korea; parkdy004@hanyang.ac.kr
[3] Department of Smart Fab. Technology, Sungkyunkwan University, Suwon 16419, Korea
[4] Applied Research Centre, Department of Electrical and Computer Engineering, Old Dominion University, 12050 Jefferson Avenue, Newport News, VA 23693, USA
[5] Department of Energy Engineering, Hanyang University, Seoul 04763, Korea
* Correspondence: seonglim@skku.edu (S.-C.L.); gnamkoon@odu.edu (G.N.); mjeong@hanyang.ac.kr (M.-S.J.)
† These authors contributed equally to this work.

Abstract: In this study, we fabricated and characterized uniform multi-cation perovskite $FA_xMA_{1-x}PbI_3$ films. We used the dynamic spin-coating method to control the cation ratio of the film by gradually increasing the FA+, which replaced the MA+ in the films. When the FA+ concentration was lower than xFA ~0.415 in the films, the stability of the multi-cation perovskite improved. Above this concentration, the film exhibited δ-phase $FAPbI_3$ in the $FA_xMA_{1-x}PbI_3$ films. The formation of δ-phase $FAPbI_3$ disturbed the homogeneity of the photoluminescence spatial distribution and suppressed the absorption spectral bandwidth with the increasing bandgap. The precise control of the cation ratio of multi-cation perovskite films is necessary to optimize the energy-harvesting performance.

Keywords: cation exchange; dynamic spin-coating; $FA_xMA_{1-x}PbI_3$; δ-phase $FAPbI_3$; FA cations; MA cations

Citation: Yu, H.M.; Jeong, B.-G.; Park, D.-Y.; Lim, S.-C.; Namkoong, G.; Jeong, M.-S. Investigation of Cation Exchange Behaviors of $FA_xMA_{1-x}PbI_3$ Films Using Dynamic Spin-Coating. *Materials* **2021**, *14*, 6422. https://doi.org/10.3390/ma14216422

Academic Editors: Ana Pilar Valerga Puerta, Severo Raul Fernandez-Vidal, Zhao Zhang and Umberto Prisco

Received: 1 October 2021
Accepted: 25 October 2021
Published: 26 October 2021

Publisher's Note: MDPI stays neutral with regard to jurisdictional claims in published maps and institutional affiliations.

1. Introduction

Recent studies have shown that mono-cation methylammonium lead triiodide ($CH_3NH_3PbI_3$, $MAPbI_3$) perovskite has some disadvantages, such as narrow absorption spectral bandwidths and weak long-term stability in the application of energy-harvesting devices [1–3]. A significant research effort has been made to overcome these problems by synthesizing the multi-cation materials [4,5]. For instance, blending formamidinium (FA) lead triiodide ($HC(NH2)_2PbI_3$, $FAPbI_3$) with $MAPbI_3$ partially replaces the MA with larger FA cations; thus, both the MA and the FA cations are present. The optical and structural properties are subject to changes, depending on the relative ratio of the multiple cations. For example, when the mixing of $MAPbI_3$ (1.64 eV) and $FAPbI_3$ (1.43 eV) is controlled, the bandgap is tuned to ~1.48 eV, which is within the near-infrared range [6,7]. However, the multi-cation materials require more attention to optimize their properties. At a particular mixing of the cation ratio, $FAPbI_3$ develops into two different phases: the photoactive black perovskite phase (α-$FAPbI_3$) and a yellow non-perovskite hexagonal phase (δ-$FAPbI_3$) [5,6]. However, the former can easily transform into the latter at room temperature with a significantly broad bandgap of 2.5 eV [5,6]. Therefore, formulating a multi-cation perovskite system using FA and MA cations requires a balanced ratio to obtain a multi-cation $FA_xMA_{1-x}PbI_3$ perovskite film with enhanced solar-cell efficiency; this has not been fully understood yet.

Among the several synthesis methods, static or dynamic spin-coating has been widely adopted as a facile way to obtain high-quality perovskite films [8,9]. In particular, dynamic spin-coating provides better perovskite film than the static method, which was widely used in the developing stage [9,10]. The static process involves coating the substrate with a perovskite precursor before spinning occurs, resulting in rapid evaporation of the perovskite solvents, anisotropic growth, fast crystallization, and nonuniform perovskite layers [9,10]. Conversely, dynamic spin-coating uses various perovskite precursors that continuously drop onto a rotating substrate [10]. Consequently, solvent evaporation is limited, and the intermediate phase is prolonged, resulting in better mixing of the perovskite elements. Additionally, dynamic spin-coating allows for (i) the solvent incompatibility of different precursors to be resolved; (ii) the separate optimization for each precursor and deposition step; and (iii) different deposition methods to be used for each deposition step.

Dynamic spin-coating provides a more efficient method for synthesizing uniform perovskite films, but the understanding of the synthesis mechanism is lacking when the dynamic spin-coating is applied to multi-cation perovskite systems.

In our study, we fabricated a multi-cation $FA_xMA_{1-x}PbI_3$ film at different concentrations of FA cations. We used the dynamic spin-coating method because it enabled us to control the amount and the type of organic cations effectively. By increasing the FA concentration, we characterized the multi-cation perovskite films using photoluminescence (PL) and X-ray diffraction (XRD). At an FA concentration xFA of ~0.415, the films showed a narrow bandgap and luminescence peak in PL and a narrow, full-width, half-maximum during XRD. Above this concentration, the film performance degraded with a wide bandgap of 2.5 eV, owing to the formation of δ-phase $FAPbI_3$.

2. Materials and Methods

2.1. Material and Sample Preparation

2.1.1. Preparation of Perovskite Precursor Solutions

First, the mixed perovskite precursor solution was prepared by dissolving 25 mg of FAI (Greatcell Solar (Queanbeyan, Australia)) and 12.5 mg of FAI (Greatcell Solar) in a 1 mL isopropyl alcohol (IPA) solution with 20 mg of MAI (Greatcell Solar (Queanbeyan, Australia)), respectively. In addition, 150 mg of PbI_2 (lead iodide, 99.9985%) in the mixed solvents of 220 μL dimethylformamide (DMF, Sigma-Aldrich (Seoul, Korea), anhydrous, 99.8%) and 20 μL dimethylsulfoxide (DMSO, Sigma Aldrich (Seoul, Korea)) was also prepared. These two solutions were prepared in a glove box (glove box condition, O_2: 0% and H_20: 0%). Afterwards, both solutions were applied on a hot plate at 70 °C for 24 h using magnetic stirring.

2.1.2. Fabrication of $FA_xMA_{1-x}PbI_3$ Film

The $FAMAPbI_3$ perovskite films were fabricated by a two-step, dynamic spin-coating procedure on the prepared FTO on glass substrates. The $FA_xMA_{1-x}PbI_3$ perovskite film was fabricated as follows. The FTO on the glass substrate was cleaned sequentially in an ultrasonic bath for 10 min each in acetone, DI water, and IPA, respectively. Afterwards, the PbI_2 perovskite precursor solution was coated on the FTO/glass substrate by using the dynamic spin-coating method at 3000 rpm for 30 s. As a result, the transparent yellow color of the PbI_2 thin film was formed. Then, the PbI_2 film was heated at 120 °C for 5 min on a hot plate. As a result, the yellow color of the PbI_2 film was obtained, as shown in the photo image in Figure 1. Finally, the mixed FAI–MAI solution of 50 μL was continuously dropped onto the pre-coated PbI_2 films at 8 s intervals during spin-coating at 4000 rpm for 30 s, then annealed at 150 °C for 10 min in an air environment. With increasing spin-coating cycles, only $FA_xMA_{1-x}PbI_3$ films with 25 mg/mL showed a gradual color change from black to bright red, whereas the films with the 12.5 mg/mL FAI remained a black color (Figure 1).

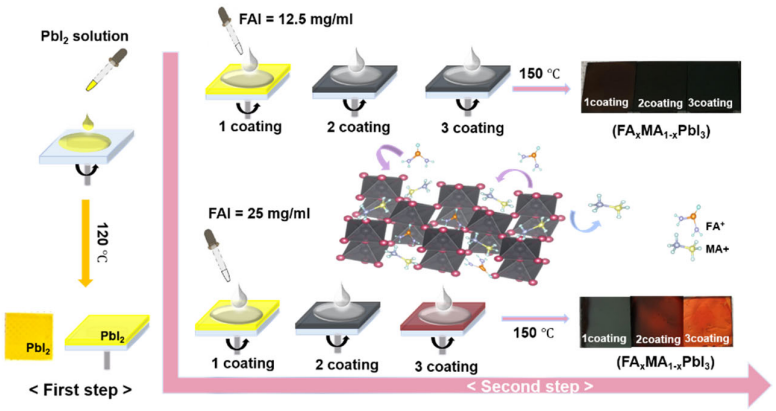

Figure 1. Synthesis of $FA_xMA_{1-x}PbI_3$ films using mixed FAI–MAI precursors.

2.2. Characterization

Field-emission scanning electron microscope (SEM) (JSM7000F) measurement was performed to investigate the surface morphologies of the $FA_xMA_{1-x}PbI_3$ films. The SEM uses a Schottky-type field-emission gun for the electron source and state-of-the-art computer technology for the image-display system. The X-ray diffraction measurements were performed using an X-ray diffractometer (Rigaku, SmartLab) with Cu-Kα radiation (λ = 1.54059 Å). The samples were scanned from 2.5° to 20° at a scan rate of 4°/min with a step size of 0.02°. The optical properties were investigated using an optical microscope system (NT-MDT) with the high-magnification objective lens (NA = 0.7). The excitation laser wavelength of 405 nm and the gratings with 150 grooves were used for the PL spectra of the perovskite films. Moreover, an ultraviolet-visible (UV–Vis) absorption spectrometer [JASCO V-670] was used to measure the chemical properties of the $FA_xMA_{1-x}PbI_3$ films.

3. Results

Figure1a describes a schematic diagram of the two-step, dynamic spin-coating method of $FA_xMA_{1-x}PbI_3$ film using the mixed FAI–MAI precursor solution. The dynamic spin-coating technology was used for continuous dispensing of the precursor solutions rather than static dispensing. In addition, for the two-step method, the amount and composition of the organic cations that can finally be incorporated into the inorganic PbX_6 (X = I-, Br-, Cl-) octahedral frameworks are determined by the intercalation capabilities of the organic cations. In the first step, PbI_2 thin films were then obtained by dropping the mixed precursor solution by spin-coating at 3000 rpm for 30 s. Subsequently, the PbI_2 films were annealed at 120 °C for 5 min in an air environment, and the color of the film turned yellow. In the second step, the mixed FAI–MAI solution was continuously dropped on the pre-coated PbI_2 film at 8 s intervals during spin-coating at 4000 rpm for 30 s and was subsequently annealed at 150 °C for 10 min. With the increasing spin-coating cycles, only the $FAMAPbI_3$ films with 25 mg/mL showed a gradual color change from black to bright red, whereas the films with the 12.5 mg/mL of FAI remained a black color (Figure 1).

To investigate the film morphology, we conducted scanning electron microscopy (SEM, Figure 2a–g). The film morphologies from the lower FAI concentration (Figure 2a–c) varied from 180 to approximately 320 and 370 nm on average for the following coatings. With increasing grain size, the film morphology roughened (Figure 2a–c). For the $FA_xMA_{1-x}PbI_3$ films with 25 mg/mL of FAI (Figure 2d–f), the average grain size increased from 160 to 320 nm and 350 nm for successive coatings. In contrast to the similar grain sizes of the films at different concentrations, the morphology was somewhat different. The $FA_xMA_{1-x}PbI_3$ film surface with a higher concentration presented wide crevasses between the grains, providing a path for ionic exchange between the FA and MA ions (this will be explained later).

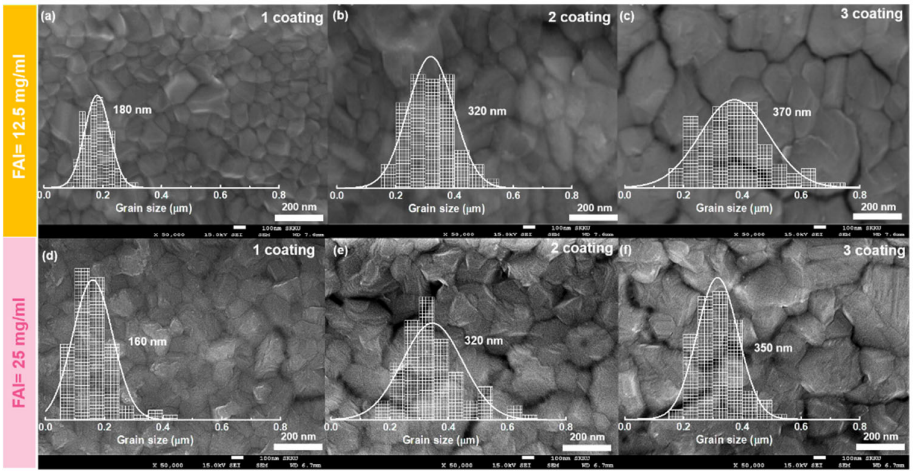

Figure 2. SEM images and grain-size distribution of $FA_xMA_{1-x}PbI_3$ films with 12.5 mg/mL FAI after (**a**) 1, (**b**) 2, and (**c**) 3 coatings and with 25 mg/mL FAI after (**d**) 1, (**e**) 2, and (**f**) 3 coatings. The scale bar is 200 nm.

XRD and UV–Vis spectroscopy were performed to investigate the ionic exchanges in the $FA_xMA_{1-x}PbI_3$ films. Figure 3a,b shows the XRD patterns of the $FA_xMA_{1-x}PbI_3$ films. After the first coating for the FAI of 12.5 and 25 mg/mL, we observed multiple XRD peaks indexed to the (100), (110), (111), (220), and (200) planes of $FAMAPbI_3$ [10]. Additionally, we observed the presence of PbI_2 at a scattering angle of 12.62°, indicating an incomplete conversion of PbI_2 to $FAMAPbI_3$ [11]. After the second coating, the PbI_2 XRD peak completely disappeared for the 12.5 and 25 mg/mL of FAI. After the third coating, a different structural phase emerged at 12.00°. The peak is responsible for the yellow phase δ-$FAPbI_3$, which is consistent with the results of a previous study [11]. To estimate the fraction of FA ratio in the perovskite film, we used the shift of diffraction peak position, and the estimation of the x value was around 0.4. The emerging yellow phase δ-$FAPbI_3$ films were also examined using UV–Vis spectroscopy (Figure 3d). For both FAI concentrations, band-edge absorption peaks of $FA_xMA_{1-x}PbI_3$ were observed at approximately 760–810 nm (Figure 3c,d) [10]. The bandgap of perovskite is changed indirectly by the mixing ratio of the organic cations because the band structure of perovskite consists of orbitals from Pb and halide [12]. Therefore, we confirmed that the slight change in bandgap of $FAMAPbI_3$ of FAI = 12.5 and 25 mg/mL using Tauc-plot (Supplement Figure S1). Interestingly, a new absorption peak near 560 nm (2.21 eV) appeared only after the third coating at an FAI of 25 mg/mL (Figure 3d). Because of its energy, δ-$FAPbI_3$ is called the yellow phase [13] and is expected to form at FA-rich concentrations.

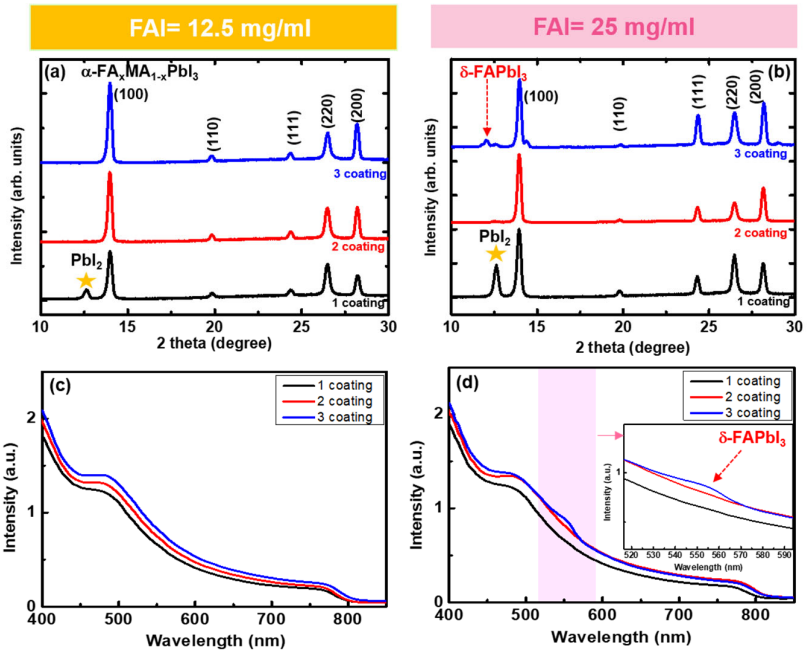

Figure 3. (**a**,**b**) XRD patterns of $FA_xMA_{1-x}PbI_3$ from 1 to 3 coatings with FAI = 12.5 and 25 mg/mL, respectively. Absorption spectra with (**c**) 12.5 and (**d**) 25 mg/mL FAI. The inset shows enlarged absorption spectra.

In addition, PL spectroscopy was performed to further elucidate the compositional changes of the $FAMAPbI_3$ film. For the first coating of $FAMAPbI_3$ film with FAI = 12.5 mg/mL, the PL peak appeared at 786 nm, which comes from the cubic α-$FAMAPbI_3$ phase [10]. As the number of coating cycles increased, the PL peaks shifted to the longer wavelengths of 790 nm in the fourth cycle of coating. The red shift in wavelengths may be due to the higher incorporation of FA cations into the $FAMAPbI_3$ film, resulting in the FA-rich α-$FAMAPbI_3$ films (Figure S2a). Interestingly, the PL intensity decreased as the number of coating cycles increased. The PL intensity of the first cycle of coating with $FAMAPbI_3$ film was the highest among all the samples with FAI = 12.5 mg/mL (Figure S2b~e). It suggests that FA-rich $FAMAPbI_3$ is accompanied by defects that increase the non-radiative recombination.

In the case of the FAI of 25 mg/mL, homogeneous spectral peaks and intensities were observed in the $FAMAPbI_3$ films with one coating (Figure 4a). No significant differences were observed up to the second coating (not shown). Conversely, in the case of three coatings with the FAI of 25 mg/mL, non-uniform spatial distribution of the PL spectra is shown, as in Figure 4c. In addition, a new PL peak appeared at 589 nm, and the inhomogeneity in the PL mapping increased (Figure 4c). There were two peaks at 589 and 765 nm (Figure 4e). The former corresponded to δ-$FAPbI_3$ [14], and the latter was represented by a blue shift of the original peak at 795 nm (Figure 4d). Increasing the FA content induced a new phase in the $FA_xMA_{1-x}PbI_3$ films. During dynamic spin-coating, the MA+ and FA+ will possibly compete for incorporation into the PbI_6 octahedral cages for nucleation [10]. A smaller amount of MA than FA cations is initially advantageous for infiltration. However, $FAPbI_3$ has a significantly lower enthalpy value (ΔH_{FAPbI3} = −4.62 eV) than $MAPbI_3$ (ΔH_{MAPbI3} = −0.149 eV) [10]. Therefore, with an increase in the number of coating cycles, the surrounding FA+ on the film surface energetically replaces the MA+, forming FA-rich α-$FAPbI_3$ perovskite. Subsequently, the energetically favorable δ-$FAPbI_3$ overpopulates α-$FAPbI_3$ in the films. The formation energy values of δ-$FAPbI_3$ and α-$FAPbI_3$ are −6.03 and −5.98 eV, respectively [15–17].

To estimate the optimum FA cation concentration xFA, which does not introduce δ-$FAPbI_3$, we analyzed the variation in the lattice constant of $FA_xMA_{1-x}PbI_3$ using XRD by gradually adding FA cations to the films. The estimated distance of the (100) crystal plane, d, of $FA_xMA_{1-x}PbI_3$ was 6.330 Å (Figure 3a). By introducing additional FA cations, the distance was modulated and scaled as $d(x) = 6.312 + 0.054 \times FA$ (Å) [10,16,17]. Our calculations revealed that the maximum FA cation concentration without δ-$FAPbI_3$ was xFA ~0.415.

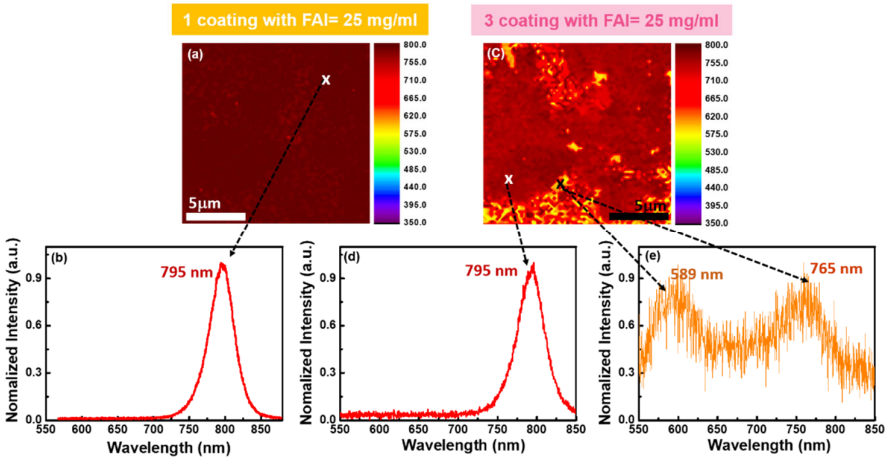

Figure 4. (**a**) PL mapping and (**b**) PL spectra of α-$FAMAPbI_3$ with 1 coating of FAI = 25 mg/mL; (**c**) PL mapping of 3 coatings of FAI = 25 mg/mL; corresponding nonuniform PL spectra of (**d**) α-$FAMAPbI_3$ and (**e**) showing δ-$FAPbI_3$ and FA-rich α-$FAMAPbI_3$.

4. Conclusions

We regulated the cation exchange of $FA_xMA_{1-x}PbI_3$ films using a dynamic spin-coating method and assessed the effect of the FA concentration on the bandgap modulation. Uniform $FA_xMA_{1-x}PbI_3$ films were fabricated using FA concentrations lower than xFA ~0.415, whereas a higher FA composition (xFA > 0.415) resulted in the introduction of δ-$FAPbI_3$ into the $FA_xMA_{1-x}PbI_3$ films. Our findings attempted to produce perovskite films with more suitable band gaps for Shockley–Queisser limits without the addition of bromide ions. The $FA_xMA_{1-x}PbI_3$ film also shows uniform morphology without forming a δ-phase $FAPbI_3$, which is of great significance in suggesting a method in which our results can produce an absorber layer to increase the efficiency of the perovskite solar cells.

Supplementary Materials: The following are available online at www.mdpi.com/1996-1944/14/21/6422/s1 Figure S1: The bandgap of $FAMAPbI_3$ of FAI = 12.5 and 25 mg/mL using Tauc-plot. Figure S2: PL spectra of $FAMAPbI_3$ of FAI=12.5 mg/ml.

Author Contributions: Conceptualization, Data curation, Formal analysis, Investigation, Methodology, Writing-original draft, Writing-review and editing, H.M.Y.; Conceptualization, Data curation, Formal analysis, Investigation, Methodology, B.-G.J.; H.M.Y and B.-G.J. contributed equally to this work. Writing-original draft and Investigation, D.-Y.P. Conceptualization, Funding acquisition, Project administration, Resources, Supervision, Validation, Writing-original draft, writing—review and editing, S.-C.L., G.N and M.-S.J. All authors have read and agreed to the published version of the manuscript.

Funding: This research was supported by the National Research Foundation of Korea (NRF) funded by the Ministry of Science and ICT (NRF-2019M3D1A1078299 and NRF-2019R1A2B5B02070657); and the Brain Pool Program [grant number 2020H1D3A2A01064555]; and the NSF [grant number 1547771]. And This work was supported by the Technology Innovation Program (or Industrial Strategic Technology Development Program (20002483, and 20011630) funded By the Ministry of Trade, Industry & Energy (MOTIE, Korea)

Institutional Review Board Statement: Not applicable.

Informed Consent Statement: Not applicable.

Data Availability Statement: In this section, please provide details regarding where data supporting reported results can be found, including links to publicly archived datasets analyzed or generated during the study. Please refer to suggested Data Availability Statements in section "MDPI Research Data Policies" at https://www.mdpi.com/ethics (accessed on 25 October 2021). You might choose to exclude this statement if the study did not report any data.

Conflicts of Interest: The authors declare no conflict of interest.

References

1. Jung, H.S.; Park, N.G. Perovskite solar cells: From materials to devices. *Small* **2015**, *11*, 10–25.
2. Hao, F.; Stoumpos, C.C.; Chang, R.P.H.; Kanatzidis, M.G. Anomalous band gap behavior in mixed Sn and Pb perovskites enables broadening of absorption spectrum in solar cells. *J. Am. Chem. Soc.* **2014**, *136*, 8094–8099.
3. Kim, H.-S.; Lee, C.-R.; Im, J.-H.; Lee, K.-B.; Moehl, T.; Marchioro, A.; Moon, S.-J.; Humphry-Baker, R.; Yum, J.-H.; Moser, J.E.; et al. Lead iodide perovskite sensitized all-solid-state submicron thin film mesoscopic solar cell with efficiency.exceeding 9%. *Sci. Rep.* **2012**, *2*, 591.
4. Eperon, G.E.; Stranks, S.D.; Menelaou, C.; Johnston, M.B.; Herz, L.M.; Snaith, H.J. Formamidinium lead trihalide: A broadly tunable perovskite for efficient planar heterojunction solar cells. *Energy Environ. Sci.* **2014**, *7*, 982–988.
5. Koh, T.M.; Fu, K.; Fang, Y.; Chen, S.; Sum, T.C.; Mathews, N.; Mhaisalkar, S.G.; Boix, P.P.; Baikie, T. Formamidinium-Containing Metal-Halide: An Alternative Material for Near-IR Absorption Perovskite Solar Cells. *J. Phys. Chem. C* **2014**, *118*, 16458–16462.
6. Luis, K.O.; Emilio, J.J.-P.; Yabing, Q. Progress on Perovskite Materials and Solar Cells with Mixed Cations and Halide Anions. *ACS Appl. Mater. Interfaces* **2017**, *9*, 30197–30246.
7. Targhia, F.F.; Jaliliab, Y.S.; Kanjouric, F. $MAPbI_3$ and $FAPbI_3$ perovskites as solar cells: Case study on structural, electrical and optical properties. *Results Phys.* **2018**, *10*, 616–627.
8. Fan, P.; Gu, D.; Liang, G.-X.; Luo, J.-T.; Chen, J.-L.; Zheng, Z.-H.; Zhang, D.-P. High-performance perovskite $CH_3NH_3PbI_3$ thin films for solar cells prepared by single-source physical vapour deposition. *Sci. Rep.* **2016**, *6*, 29910.
9. Bing, J.; Kim, J.; Zhang, M.; Zheng, J.; Lee, D.S.; Cho, Y.; Deng, X.; Lau, C.F.J.; Li, Y.; Green, M.A.; Huang, S.; Ho-Baillie, A.W.Y. The Impact of a Dynamic Two-Step Solution Process on Film Formation of $Cs_{0.15}(MA_{0.7}FA_{0.3})_{0.85}PbI_3$ Perovskite and Solar Cell Performance. *Small* **2019**, *15*, 1804858.
10. Jung, K.; Lee, J.-H.; Oh, K.; Im, C.; Do, J.; Kim, J.; Chae, W.-S.; Lee, M.-J. Efficient composition tuning via cation exchange and improvedreproducibility of photovoltaic performance in $FA_xMA_{1-x}PbI_3$ planarheterojunction solar cells fabricated by a two-step dynamic spin-coatingprocess. *Nano Energy* **2018**, *54*, 251–263.
11. Chen, Z.; Zhang, H.; Yao, F.; Tao, C.; Fang, G.; Li, G. Room Temperature Formation of Semiconductor Grade α-$FAPbI_3$ Films for Efficient Perovskite Solar Cells. *Cell Rep. Phys. Sci.* **2020**, *1*, 100205.
12. Filip, M.R.; Eperon, G.E.; Snaith, H.J.; Giustino, F. Steric engineering of metal-halide perovskites with tunable optical band gaps. *Nat. Comm.* **2014**, *5*, 5757.
13. Jana, A.; Ba, Q.; Nissimagoudar, A.S.; Kim, K.S. Formation of a photoactive quasi-2D formamidinium lead iodide perovskite in water. *J. Mater. Chem. A* **2019**, *7*, 25785–25790.
14. Ma, F.; Li, J.; Li, W.; Li, N.; Wang, L; Jia, Z.; Xue, J.; Qiao, J. Stable α/δ phase junction of formamidinium lead iodide perovskites for enhanced near-infrared emission. *Chem. Sci.* **2017**, *8*, 800–805.
15. Park, B.; Kwon, H.; Lee, Y.; Lee, D.; Kim, M.; Kim, G.; Kim, K.-j.; Kim, Y.K.; Im, J.; Shin, T.J.; Seok, S.I. Stabilization of formamidinium lead triiodide α-phase with isopropylammonium chloride for perovskite solar cells. *Nat. Energy* **2021**, *6*, 419–428.
16. Weller, M.T.; Weber, O.J.; Frost, J.M.; Walsh, A. Cubic perovskite structure of black formamidinium lead iodide, α-$[HC(NH_2)_2]PbI_3$, at 298 K. *J. Phys. Chem. Lett.* **2015**, *6*, 3209–3212.
17. Weber, O.J.; Charles, B.; Weller, M.T. Phase behaviour and composition in the formamidinium–methylammonium hybrid lead iodide perovskite solid solution. *J. Mater. Chem. A* **2016**, *4*, 15375–15382.